In vitro investigation of the photoprotection mechanism of Light Harvesting Complex II

Crisafi, E.

CHAPTER 5

NMR studies on ^{13}C lutein- rLhcb1

ABSTRACT

We applied selective lutein ^{13}C isotope labelling to study the structure and plasticity of the two luteins in the Light-Harvesting Complex II (LHCII) pigment-protein complex. In Chapter 4 we used recombinant expression and pigment reconstitution for selective isotope pigment labelling, allowing us to obtain selective ^{13}C labelled lutein monomeric LHCII using recombinant monomeric Lhcb1 from *A. thaliana* without the signals coming from the protein amino acids or from other carotenoids, Chls or lipids. In this chapter, we investigate the structure and dynamics of the two luteins in LHCII in with high-resolution Magic Angle Spinning (MAS) NMR. The pigment-protein complex is prepared in detergent micelles or in the aggregated state [1,2], in which the protein respectively forms fluorescent and fluorescence-quenched states.

Our results show that we, for the first time, could obtain structural information of the luteins in LHCII in the unquenched, fluorescent state, which is not accessible by X-ray crystallography. By analysis of ^{13}C-^{13}C and ^{1}H-^{13}C correlation NMR spectra we could obtain NMR ^{13}C chemical shift assignments of the lutein head atoms.

INTRODUCTION

Carotenoids in photosynthesis are essential both for increasing the light-harvesting absorption range and for photoprotection against photodamage. Among the pool of photosynthetic pigments in plants, the lutein counts for the 60% of the xanthophylls and the 40% of all the carotenoids, which makes this pigment the most abundant xanthophyll species [3]. Lutein has a structural role in the stability of Light-Harvesting Complexes (LHCs) and his presence is essential for correct folding of the proteins [3-5]. *In vitro* reconstitution shows that the lack of lutein *per se* is sufficient to prevent trimerization [3]. Carotenoid triplets have a photoprotective role in quenching long-lived $^{3}Chl^{*}$, which can react with O_2 forming harmful singlet oxygen [3]. In higher plants, recent studies show that lutein is involved in a lutein epoxidation (LutE) cycle which converts lutein to epoxidase lutein. Both reactions of the LutE cycle are catalysed by the violaxanthin de-epoxidase enzyme (VDE) and zeaxanthin epoxide (ZEP), which are involved as well in more well-known violaxanthin cycle [6].

LHCs protein of plants and algae are responsible for sunlight absorption and under moderate light conditions, transfer excitations to the reaction center. Instead, in the presence of intense light, LHCs associated with Photosystem II dissipate the excess of light energy to prevent photodamage by rapid quenching of excitations. The LHC proteins, of which Light-Harvesting Complex II is the most abundant, have the intrinsic property to alternate between light-harvesting, fluorescent and photoprotective, quenched states by reversible switching of their conformations [7,8].

The molecular mechanism that triggers the photoprotective switch of the protein has not been resolved yet [9-12]. In LHCII, Lut1, which occupies the L1 site, has been proposed to function as a quencher in the photoprotective state. This lutein is close to Chl *a*610, Chl *a*611 and Chl *a*612 that are the reddest Chls in LHCII [3]. Because these Chls have the lowest excitation energy [3], excitations will accumulate here and this site is assumed to be the site of energy dissipation in the photoprotective state. The switch into a photoprotective state has been proposed to involve a change in the interaction between lutein and those Chls, producing a quenched state via energy transfer from the Chls to the Cars S1 state, or via Chl-Cars excitonic interactions [11].

Lut1 is also involved in energy transfer to Chl *a* in light-harvesting conditions [9], and its presence is required for efficient Chl triplet quenching as demonstrated by Dall' Osto *et al.* [3].

The presence of lutein in the L1 site is essential since the non-occupancy of site L2 did not significantly affect photobleaching in recombinant LHCII [5,13].

In this chapter, we explore the role of lutein in the conformational switch of LHCII by comparing the lutein conformations in fluorescent and quenched LHCII states. Hereto, rLhcb1 from *A. thaliana* has been refolded in the presence of ^{13}C labeled lutein together with all the other pigments unlabeled. This selective labelling strategy allows to simplify the NMR spectra and concentrate specifically on the lutein signals. We mimic LHCII in unquenched and quenched state, by preparing the protein in detergent solution (*β*-DM) and in the aggregated state. In the aggregated state, the LHCII proteins interact with each other, which is known to produce quenched states as reported in Chapter 2. To reveal

the lutein conformational structures and understand how the lutein pigment molecules interact with their environment, we perform a MAS NMR study on ^{13}C lutein-rLhcb1. In Figure 5.1, we take a closer look into the LHCII protein, highlighting the two luteins (in orange), which are sandwiched between the transmembrane-helices A and B.

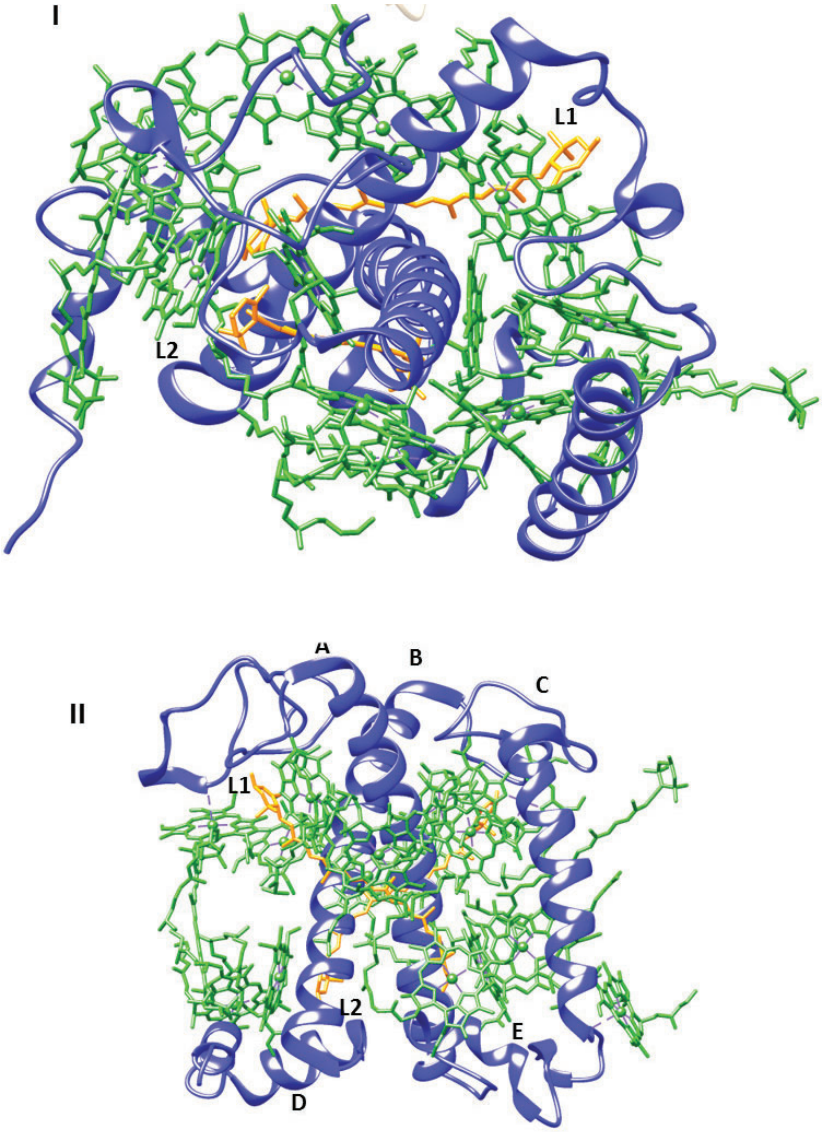

Figure 5.1 The top and side view of LHCII from spinach (PDB-1RWT) are respectively I and II. In green all the Chls, Neo and Vio are presented while in orange the luteins are presented (L1 and L2 accordingly to nomenclature of Standfuss et al. [14]).

The two X-ray structures that have been published of LHCII in 2004 and 2005, by Liu *et al.* and by Standfuss *et al.* respectively, have a resolution of 2.75 Å and 2.5 Å [14,15]. This resolution is not enough to determine atomic bond lengths, and for instance, distinguish between the chemical structures of the two lutein heads. With NMR spectroscopy, in contrast, it is possible to distinguish between signals from the two head groups because of the different position of the double bonds. Another advantage of NMR over X-ray crystallography is the possibility to investigate samples in different physical states, *i.e.*

liquid, solid, gel like, *etc*. This is an enormous advantage if we consider that for X-ray the sample should be crystallized and that long-range crystalline order is required. LHCII in crystalline form adopts a quenched like state which per definition does not give opportunity to study its conformational switch [10,16]. With NMR instead, we can prepare samples in different conditions to reproduce the two switch states. Furthermore NMR, in general, offers the possibility of probing samples at a wide range of temperatures, which helps to determine dynamic features of molecules.

MATERIALS AND METHODS

SAMPLE PREPARATION

DETERGENT SAMPLE PREPARATION

The preparation of recombinant Lhcb1 with ^{13}C lutein has been described in Chapter 4. All the purified fractions, previously characterized and stored at -80°C, were combined together for characterization by NMR. The total sample volume was concentrated, using Corning Spin-X UF 20 ml concentrators with 10 kDa pore size. The final volume was 150 µl and the sample was split in two fractionss. One fraction was used to mimic the unquenched state of rLhcb1 by solubilizing the protein in β-DM detergent. 70 µl of this sample were loaded in a 4mm rotor, which corresponded to ~6 mg Chl (*a*+*b*). The sample was carefully packed in the rotor via several short spinning steps.

AGGREGATE SAMPLE PREPARATION

The remaining sample was used to mimic the quenched state via protein aggregation. Pandit *et al.* showed that aggregated LHCII after detergent removal remains its tertiary structure because the pigment-protein complexes have a comparable NMR profiles [2].
As already demonstrated in previous work, in result of the detergent dilution, LHCII aggregates are formed, and the consequent dramatic decrease in the fluorescence of LHCII was shown to resemble, in several aspects, the *in vivo* NPQ state [7,17,18].
The ^{13}C lutein-rLhcb1 sample was diluted until the detergent concentration was below the critical micelle concentration (CMC). The CMC of *β*-DM detergent in water is around 0.17 mM which corresponds with 0,0087 % [19]. This means that in order to aggregate the protein, the final concentration of *β*-DM should be at least less than the CMC above indicated. To achieve the aggregation state, the protein sample was diluted accordingly. The sample was concentrated using the same Corning Spin-X UF 20 ml concentrators used as described above. The volume sample was reduced to 2 ml and dialyzed against 3 L of HEPES buffer, 0.01 M, devoid of detergent. Finally, the aggregated sample was successfully pelleted by ultracentrifugation (Optima L, Beckman Coulter). By adding of few microliters of the buffer, the solid aggregates could be transferred to the 4 mm rotor. The sample was packed using short spinning steps as described above.

UV-VIS ABSORPTION

UV-Vis measurements were performed with a Cary 60 spectrophotometer (Agilent technologies). Spectra were collected between 350 nm and 750 nm using 0,1 or 1 cm quartz cuvettes.

TIME RESOLVED FLUORESCENCE

Time-resolved fluorescence measurements were performed using a FluoTime 300 (PicoQuant) time-correlated photon counter spectrometer. Samples were held in a 1x1 cm quartz cuvette that was thermostated at 20°C and excited at 440 nm using a diode laser (PicoQuant). Fluorescence decay traces were fitted with a multi-exponential decay curve using a χ^2 least-square fitting procedure.

NMR EXPERIMENTS

NMR measurements were performed on a Bruker avance-I 750 MHz wide bore solid-state NMR spectrometer with 17.6 Tesla magnetic field. In this field, ^{13}C and ^{1}H resonate at 188.66 and 750.23 MHz respectively. Standard 4mm triple resonance MAS probe was used for the experiments. All the samples were packed in 4mm zirconium rotors with a spacer and top insert and were spun at the magic angle (54.74°) at a spinning frequency of 14 kHz. The temperature was kept constant at 220 K.

Approximately 70 µl of sample volume containing ~ 6 mg of Chl (*a*+*b*) was loaded in the 4mm rotor.

^{13}C spectra were obtained through cross-polarization magic-angle spinning (CP-MAS) technique with SPINAL64 decoupling [20]. ^{1}H and ^{13}C were irradiated with 80.6 kHz and 62.5 kHz radio frequency pulses with a contact time of 2 ms used to achieve the CP condition. For an acquisition time of 20 ms, a recycle delay of 1 s was used and more than. The line broadening function of 50 Hz was applied while processing the spectra. All the ^{13}C spectra were externally referenced to $^{13}COOH$ resonance of *U* [^{13}C-^{15}N]-tyrosine/HCl which was referenced to tetramethylsilane (TMS). After optimizing the conditions for 1D ^{13}C CP MAS spectra, 2D ^{1}H-^{13}C HETCOR and ^{13}C-^{13}C PARIS experiments were implemented. For ^{1}H-^{13}C HETCOR, different contact times, i.e. 256 µs, 1024 µs, and 3072 µs were used. For ^{13}C-^{13}C PARIS experiments, mixing times of 10 ms, 25 ms or 30ms were used. The basis of the applied pulse sequences is explained below.

CP-MAS

Cross-Polarized Magic Angle Spinning (CP-MAS) is a technique which is applied to detect low gamma (γ) of rare nucleus such as ^{13}C or ^{15}N. Obtaining a good spectrum of low gamma nuclei is challenging due to their low abundances, low spin polarization, low signal intensity and their characteristic long relaxation times compared to protons leading to long acquisition times. All these aspects can be overcome by CP technique, where the magnetization is transferred from abundant nuclei to rare nuclei. CP is achieved via dipolar couplings and is obtained through the simultaneous application of

two external radio-frequency fields satisfying the Hartmann-Hahn condition [21]. When protons are in the proximity of ^{13}C nuclei, magnetization is transferred, which increases the sensitivity for detecting the ^{13}C nuclei, and the relaxation delays are reduced by exciting the ^{1}H and ^{13}C together with matching spin lock pulses. CP goes via dipolar coupling and is always combined with MAS. In the MAS experiment, the sample is spun rapidly in a cylindrical rotor around a spinning axis oriented at the magic angle 54.74° with respect to the applied magnetic field [22] [23]. MAS averages the hetero-nuclear dipolar coupling and chemical shift anisotropy (CSA) interactions to zero. Thus, at higher spinning speeds, the inhomogeneous anisotropic line broadenings are removed resulting in narrow central lines. Although MAS removes the main effects of the anisotropic dipolar interactions on the linewidths, higher order effects must be still removed by spin decoupling. This can be achieved through the application of radio-frequency irradiation schemes on the non-observed spins for heteronuclear interactions. Among the several techniques available for heteronuclear decoupling, small phase incremental alternation with 64 steps (SPINAL-64) has been used for the experiments described in this chapter [24].

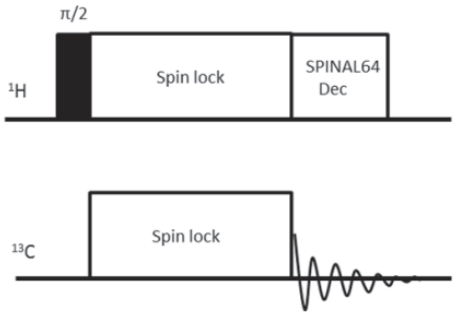

Figure 5.2 Schematic representation of CP-MAS pulse sequence.

HETCOR

Heteronuclear correlation spectroscopy (HETCOR) is a multidimensional experiment [25] that correlates heteronuclear resonances, typically ^{13}C or ^{15}N with ^{1}H resonances, by transferring polarization between the heteronuclear ^{13}C or ^{15}N and ^{1}H spins. For solids, obtaining narrow lines in the proton dimension is challenging and this is overcome by the using frequency switched Lee-Goldburg irradiation technique (FSLG) [26].

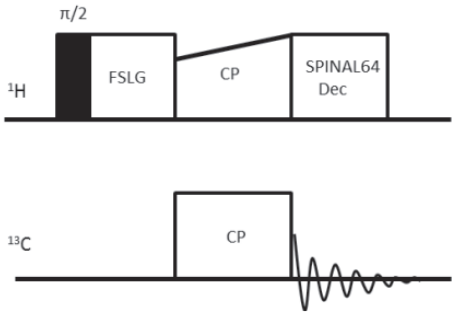

Figure 5.3 Schematic representation of HETCOR pulse sequence.

In our 2D HETCOR experiments, the indirect dimension is the proton while the direct dimension is ^{13}C. By varying the CP contact times, it is possible to get information from directly-bounded proton and carbons using shorter contact times such as 128 μs, while the longer contact times, 1072 or 3072 μs, give rises to correlated peaks coming from correlations over several bond distances.

PARIS

Phase Alternated Recoupling Irradiation Schemes (PARIS) was used as dipolar recoupling scheme in ^{13}C-^{13}C experiments.

2D ^{13}C-^{13}C correlation experiments are essential for defining the tertiary structure of proteins, through space correlation [27].

The efficiency in the magnetization transfer between two carbon nuclei during a recoupling experiment depends from several factors: spatial proximity (r), chemical shift (Δδ) and strength of ^{1}H-^{1}H dipolar couplings present in the surrounding proton bath. The last two parameters are sensitive to the specific experimental conditions that are applied [28].

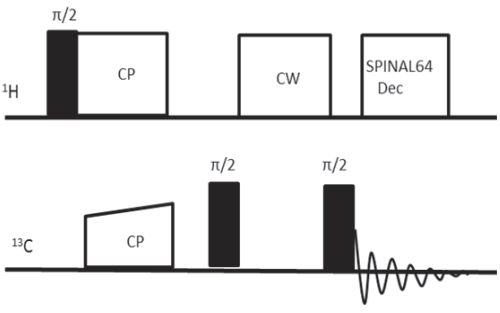

Figure 5.4 Scheme of PARIS pulse sequence.

Using short mixing time, τ_m= 10 ms, the spin diffusion, ^{13}C-^{13}C is restricted to the closest atoms, while with the increasing of τ_m= 30 ms the spin diffusion is extended to the farther atoms.

RESULTS AND DISCUSSION

The quenched and unquenched ^{13}C lutein-rLhcb1 samples were characterized by UV-Vis absorption and time-resolved fluorescence spectroscopy. The quenched sample shows some scattering in the absorption spectrum due to the aggregate particles suspended in the solution which interferes with the absorption. The samples were compared to the spectra of native LHCII monomer and trimer extracted from market fresh spinach leaves as displayed in Figure 5.5.

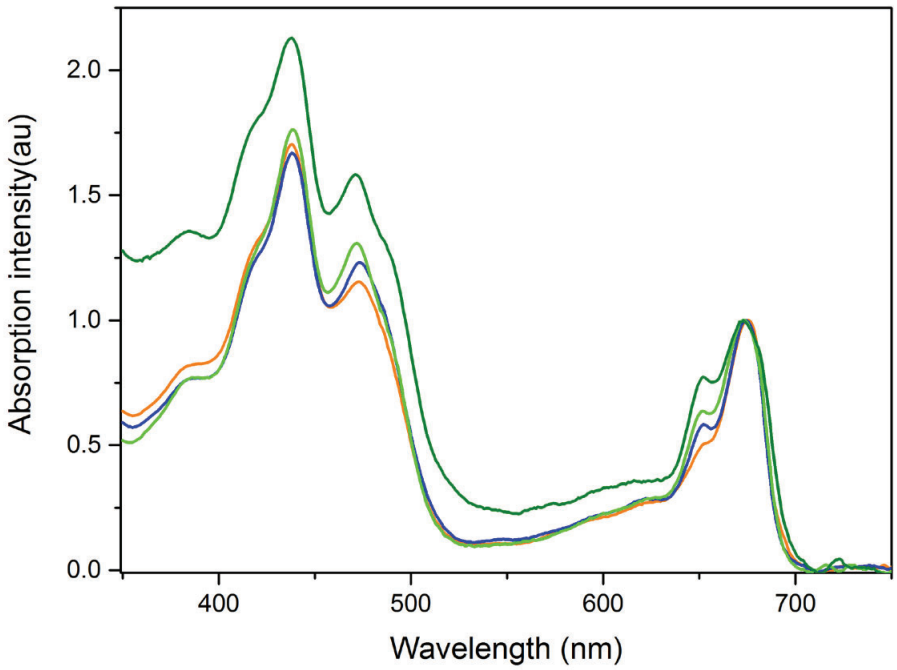

Figure 5.5 In blue LHCII trimer in β-DM, in orange LHCII monomer in β-DM, in light green ^{13}C lutein-rLhcb1 in β-DM and in dark green the ^{13}C lutein-rLhcb1 aggregate. Spectra are normalized to the intensity at 680 nm.

As shown in Figure 5.6 and Table 5.1, the Chl excited-state lifetimes are drastically reduced in aggregated ^{13}C lutein-rLhcb1 compared to detergent-solubilized ^{13}C lutein-rLhcb1, which indicates that the aggregated protein is in a strongly quenched state.

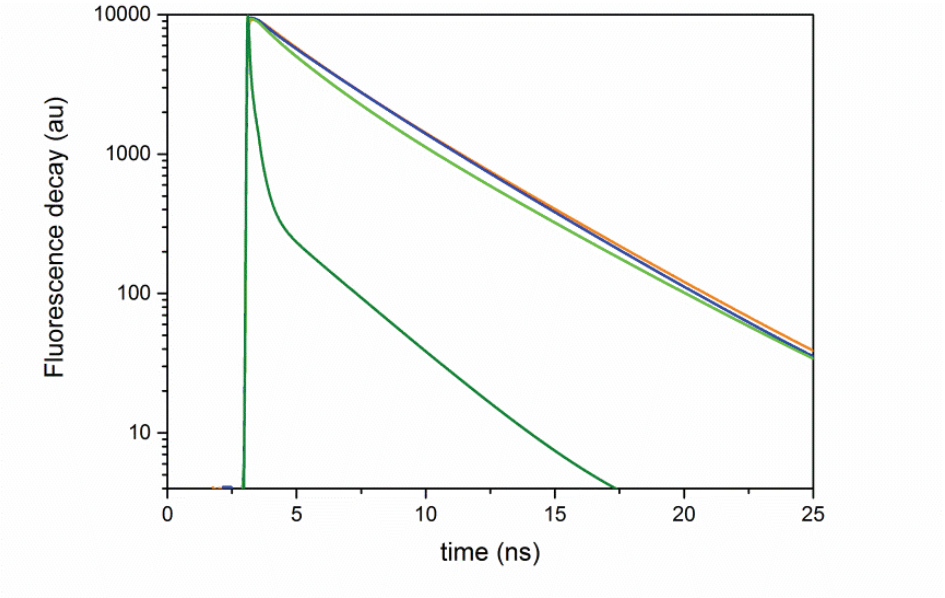

Figure 5.6 Time resolved fluorescence decay spectra. In blue LHCII trimer in β-DM, in orange LHCII monomer in β-DM, in light green ^{13}C lutein-rLhcb1 in β-DM and in dark green the ^{13}C lutein-rLhcb1 aggregate.

	A_1(%)	τ_1(ns)	A_2 (%)	τ_2(ns)	A_3(%)	τ_3(ns)	τ av(ns)
LHCII monomer	63.1	4.2	36.9	2	-	-	3.3
LHCII Trimer in β-DM	51.4	4.2	36.5	2.6	12.1	0.5	3.2
^{13}C lutein-rLhcb1 in B-DM	42.5	4.3	43.7	1.9	13.8	0.4	2.7
^{13}C lutein-rLhcb1 aggregate	38.3	0.3	55.6	0.1	6.1	2.7	0.3

Table 5.1 Fitted fluorescence lifetimes of decay traces shown in Figure 5.6.

NMR SPECTROSCOPY

1D ^{13}C CP-MAS EXPERIMENTS

Temperature dependence of ^{13}C CP-MAS NMR spectral intensities of ^{13}C lutein Lhcb1 in β-DM

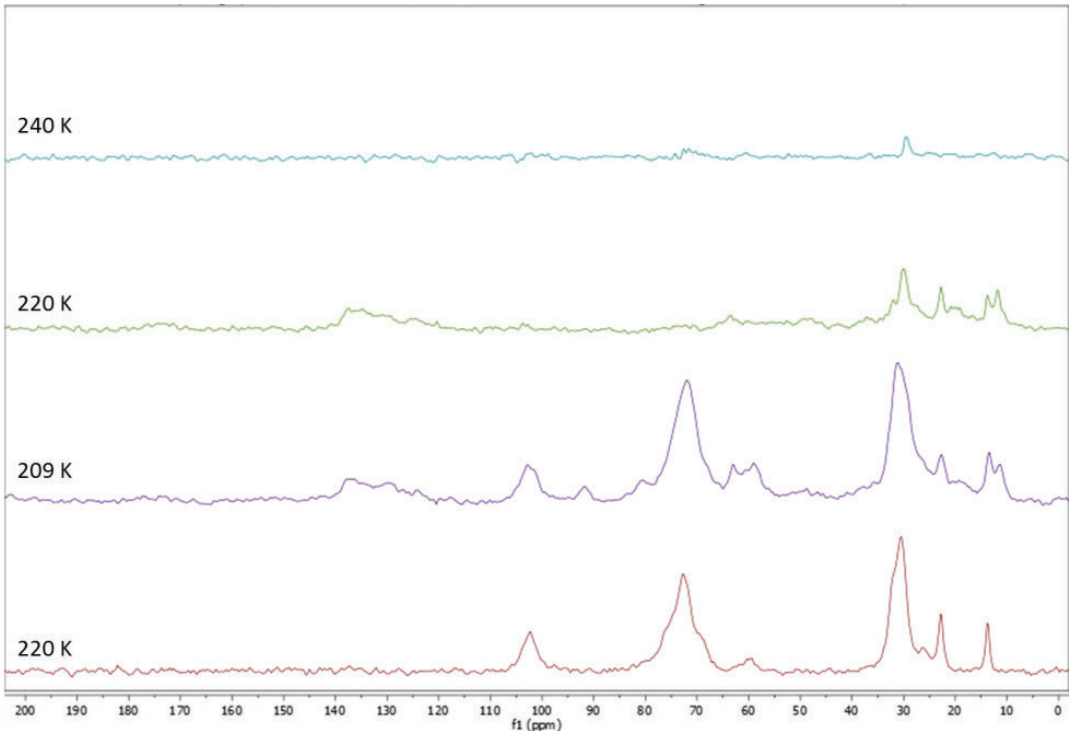

Figure 5.7 CP-MAS spectra of ^{13}Clutein-rLhcb1in βDM at 240K in blue, 220K in green, 209K in purple. The spectrum of βDM at 220K is presented in red.

For the unquenched sample, lutein ^{13}C chemical shifts are only visible if the temperature is lowered below 240 K due to dynamics of the lutein molecules that makes cross polarization inefficient because of averaging of the dipolar couplings to zero (Figure 5.7). The 1D CP-MAS spectra presented in Figure 5.7 were collected with the same number of scans (NS=512). Following the signal intensities as function of temperature, we observe that going from 240 to 220 K, signal intensities increase, from which we can conclude that the lutein dynamics is reduced. Below 220 K the signal intensities decrease again and are obscured by strong signals of the *β*-DM detergent molecules (purple spectrum) that become immobilized. Therefore, 220 K was chosen as the optimal temperature.

Comparison of the ^{13}C CP MAS NMR spectra of ^{13}C lutein-rLhcb1 in β-DM, ^{13}C lutein-rLhcb1 aggregates and ^{13}C lutein as crystalline powder.

Spectra of ^{13}C lutein-rLhcb1 in quenched and unquenched states collected at 220K are shown in Figure 5.8, together with the 1D spectrum from lutein as crystalline powder as a reference (Sigma). The spectra show that lutein -CH, $-CH_2$ and $-CH_3$ signals can be detected in the ^{13}C lutein-rLhcb1 sample in the two conditions. In the ^{13}C lutein-rLhcb1 spectra, we observe natural abundance ^{13}C signals from the protein, including the backbone -CO peak at ~175 ppm. The asterisks indicate the peaks coming from the detergent, which are clearly visible at ~100 pm and 70 ppm.

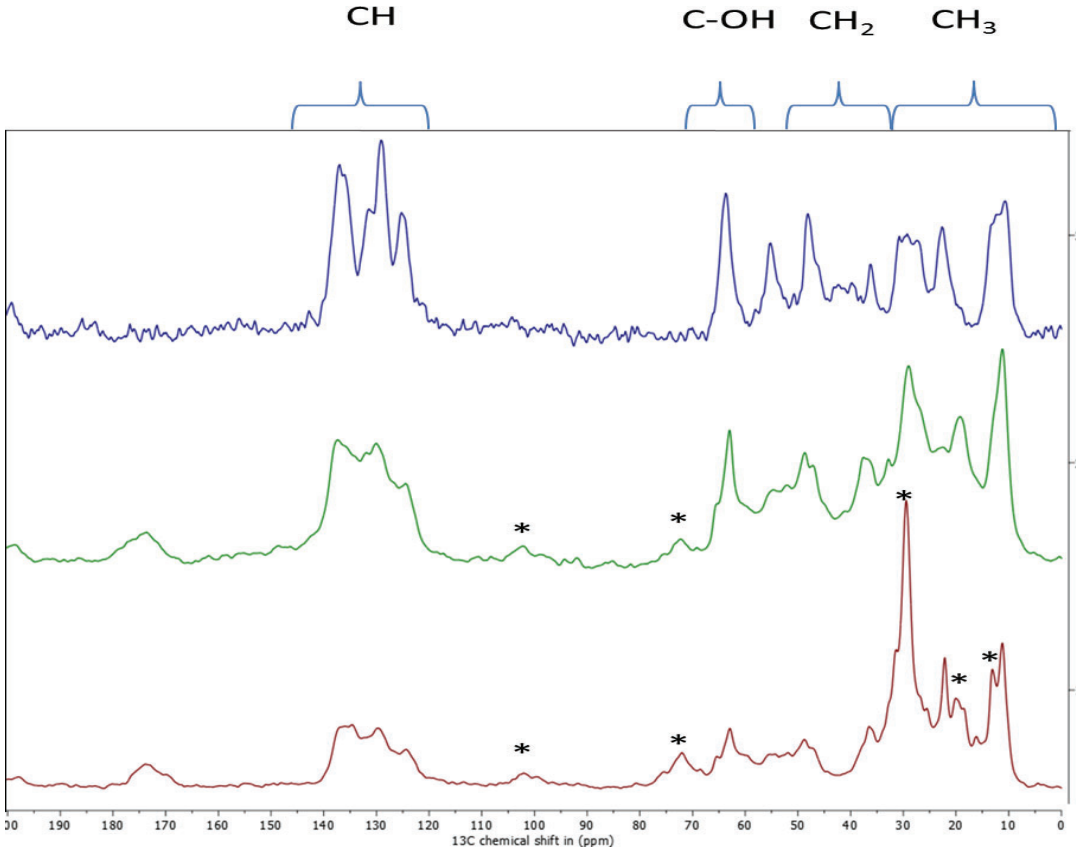

Figure 5.8 CPMAS experiment showing in blue ^{13}C lutein in crystalline form, in green the aggregate ^{13}C lutein-rLhcb1 and in red the ^{13}C lutein-rLhcb1 in β-DM. Asterisk indicate peaks from the β-DM.

^{1}H-^{13}C HETCOR NMR EXPERIMENTS

^{1}H-^{13}C HETCOR experiments of ^{13}C lutein-rLhcb1 in β-DM and of ^{13}C lutein-rLhcb1 aggregates were recorded at 220 K using different mixing times. Figure 5.9 shows the comparison of HETCOR spectra different two mixing time, 256 and 3072 µs, for the detergent sample. A similar pattern is observed for the HETCOR experiment of only lutein (data shown in Figure A5.6).

Interestingly, in the HETCOR spectra with long mixing times a narrowing of the peaks is observed, compared to the 256 µs spectrum, which is correlated with the extension of the correlations. Notably, an up-field shifted ^{1}H peak with a chemical shift around -2 ppm

(ω_1, ^{1}H), correlating with 16 ppm (ω_2, ^{13}C) is present in the HETCOR spectrum of ^{13}C lutein-rLhcb1 in β-DM with the mixing time of 256 µs that is not visible in spectra collected with longer mixing time.

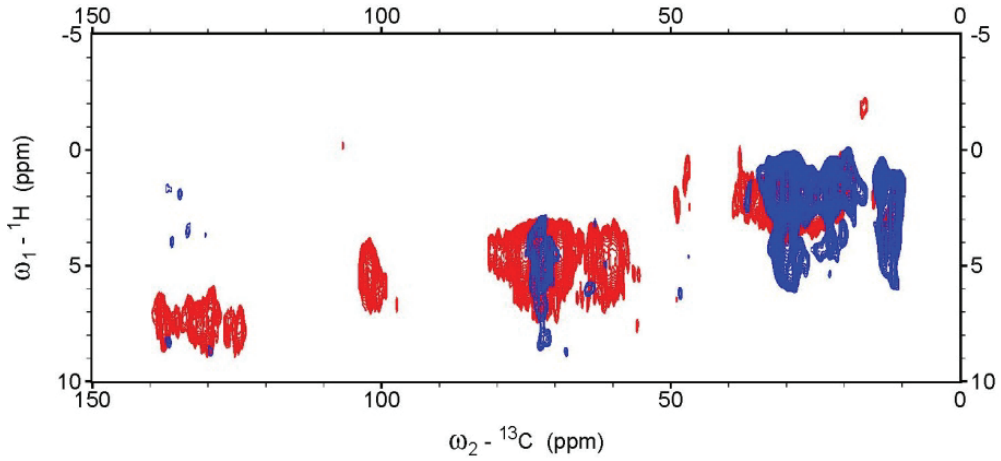

Figure 5.9 HETCOR ^{1}H-^{13}C spectra of ^{13}C lutein-rLhcb1 in β-DM collected with 256 µs mixing time (red) and with 3072 µs mixing time (blue).

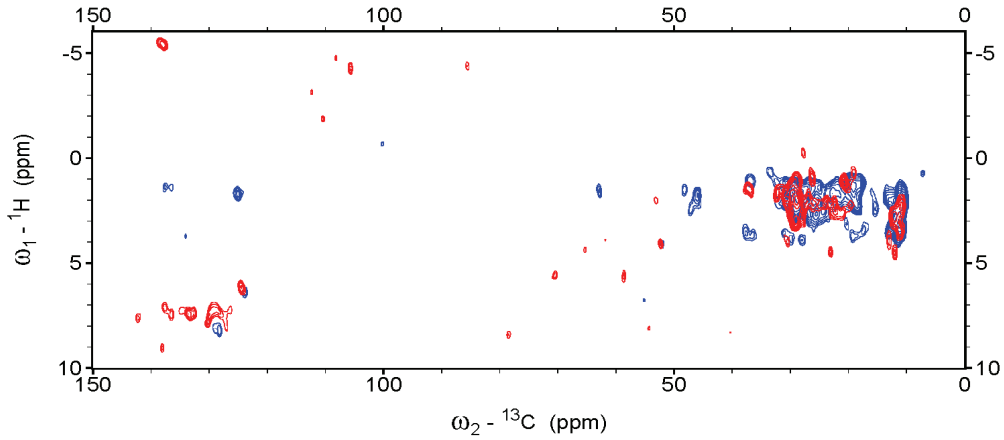

Figure 5.10 HETCOR ^{1}H-^{13}C spectra of aggregated ^{13}C lutein-rLhcb1 collected with 256 µs mixing time (red) and with 3072 µs mixing time (blue).

With the short mixing time, only one-bond correlations are observed, while with the long mixing time it can be deduced that up to three-bond correlations are observed. For instance, correlations between the acyl-chain methyl protons and -CH carbons are observed in the region between 0-5 ppm (ω_1) and 120-150 ppm (ω_2). In Figure 5.10 the HETCOR spectra of the aggregate ^{13}C lutein-rLhcb1 at short and long mixing times are overlaid. Figure 5.11 shows a comparison of the detergent and aggregate sample at 256 µs mixing time.

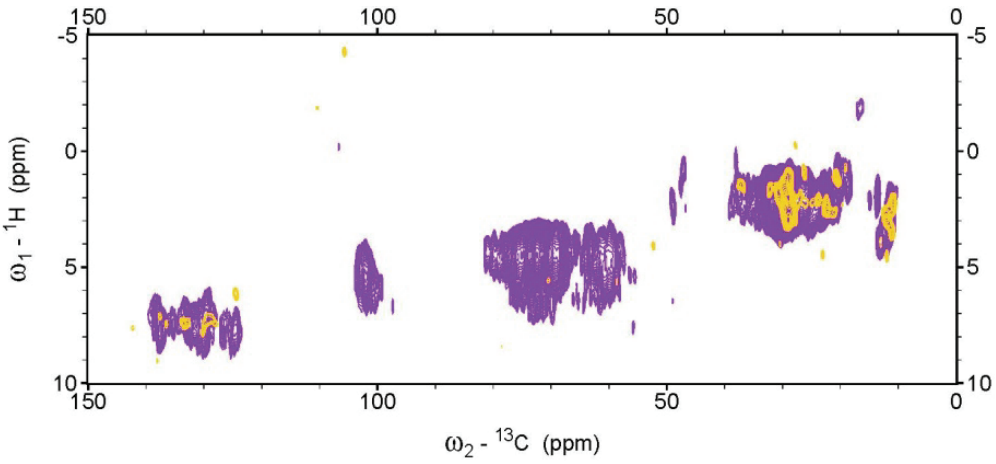

Figure 5.11 HETCOR ^{1}H-^{13}C spectra with 256 us mixing time. Spectra of ^{13}C lutein-rLhcb1 in βDM (purple) and of aggregated ^{13}C lutein-rLhcb1 (yellow).

However, the signal intensities of the aggregate sample were too weak for a proper comparison with the detergent sample and in our further analysis, we continued with the detergent sample of ^{13}C lutein-rLhcb1 in unquenched state.

Assignment of the ^{13}C lutein head atoms in ^{13}C-lutein rLhcb1 in βDM.

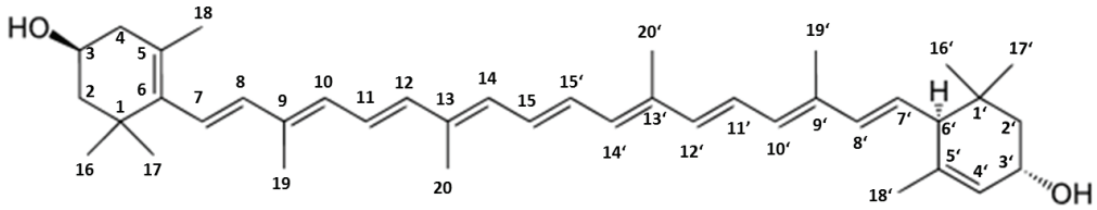

Figure 5.12 Chemical structure of lutein and atom numbering used for the assignments.

Through the combined analysis of the ^{1}H-^{13}C HETCOR and ^{13}C-^{13}C CP PARIS experiments, it has been possible to perform an assignment of the ^{13}C carbons in the lutein heads, that have better dispersion than the signals from the lutein polyene chains. The overlay of the spectrum of ^{13}C lutein-rLhcb1 in *β*-DM with the spectrum of only *β*-DM (Figure A5.3) confirms that the peaks coming from the *β*-DM detergent are not interfering with the lutein signals in the aliphatic region between 30-60 ppm and the aromatic region between 125-140 ppm.

^{13}C-^{13}C PARIS spectra of ^{13}C lutein-rLhcb1 in *β*-DM with 25 and 30 ms mixing time in combination with the HETCOR spectrum at 256 μs mixing time was used for NMR assignment of the lutein head atoms as shown in Figure 5.13 and summarized in Table 5.2.

The connections between vicinal atoms have been built starting from the peaks relative to the C18 and C18'. The lutein ^{13}C chemical shift assignments are presented in Table 5.2 and the lutein chemical structure with the atoms numbered is presented in Figure 5.12. We could distinguish the two lutein heads, owing to the double-bond character of carbons in the head-groups. For some correlations, peak doubling is observed due to the fact that the two luteins are in non-equivalent protein environments.

As mentioned above, in the HETCOR spectrum an up-field shifted peak is observed around -2 ppm. Closer inspection shows a doubling of this peak, -1.7 ppm and -2 ppm, indicating that signals of the two luteins are distinguished. We can assign the cross peaks to the -CH_3 in position C18' in the lutein head for both the luteins. The origin of this shift lies in the proximity of this methyl group of Lut1 to the ring of Chl *a*610, and of the head methyl group of Lut2 to the ring of Chl *a*602. Ring-current shifts are very sensitive to changes in the lutein orientation and therefore these NMR signals could be used as a marker in further experiments to compare lutein orientation and interactions in the unquenched and quenched state.

The -CH signals coming from the conjugated lutein chain accumulate in the region between 125-140 ppm, hampering unambiguous assignments.

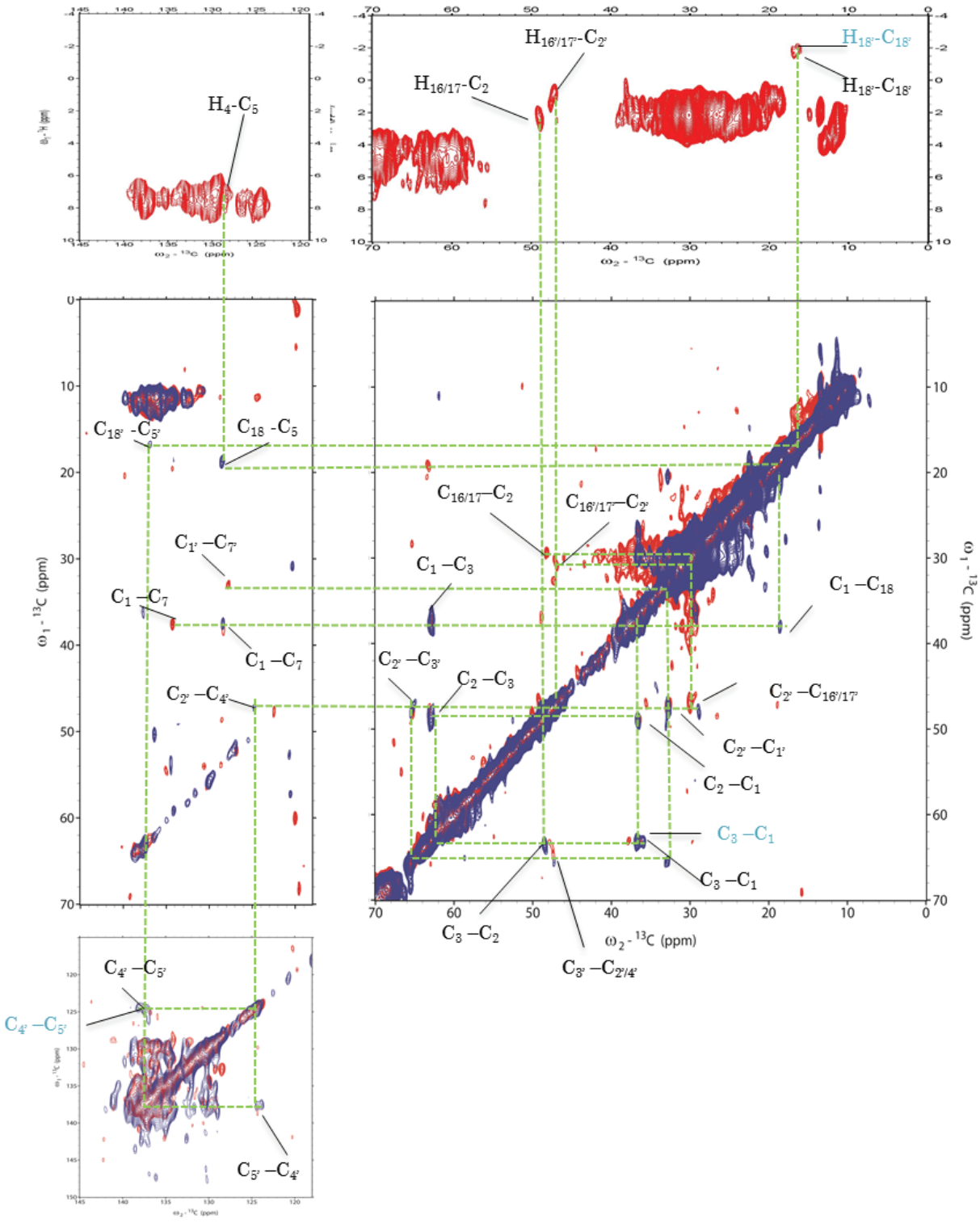

Figure 5.13 ^{13}C-^{13}C CP PARIS NMR spectra of ^{13}C lutein-rLhcb1 in βDM detergent collected with 25 ms in blue with and 30 ms in red, together with the ^{1}H-^{13}C HETCOR spectrum collected with 256 μs mixing time (in red).

Atom	i	δ	ii	δ	i'	δ	ii'	δ
C1, C1'	36.0	2.0	36.7	2.7	32.7	-4.4		
C2, C2'	48.5	2.9			47.5	-0.9		
C3, C3'	62.7	0.8			65.6	-0.3		
C4, C4'					124.5	0.0		
C5, C5'	128.5	-0.7			136.8	-0.9	136.1	-1.6
C6, C6'	134.3	-3.7						
C7, C7'	128.2	2.4			127.6	-1.1		
C16/17, C16'/17'	29.4	0.7			32.8	3.3	30.3	0.8
C18, C18'	18.9	-1.5			16.4	-6.5	16.9	-6.0

Table 5.2 ^{13}C chemical shifts of ^{13}C lutein-rLhcb1 in β-DM are compared to the chemical shifts of lutein in $CDCl_3$. i and ii represent double peaks, for carbons having different chemical shifts for the two luteins. The column identified with δ represents the chemical shift difference between the ^{13}C lutein-rLhcb1 in β-DM and lutein in $CDCl_3$.

Figure 5.14 maps the chemical-shift differences between ^{13}C lutein-rLhcb1 in β-DM and lutein in $CDCl_3$ solution and represents the influence of the protein environment on the lutein ground-state electronic structure.

.

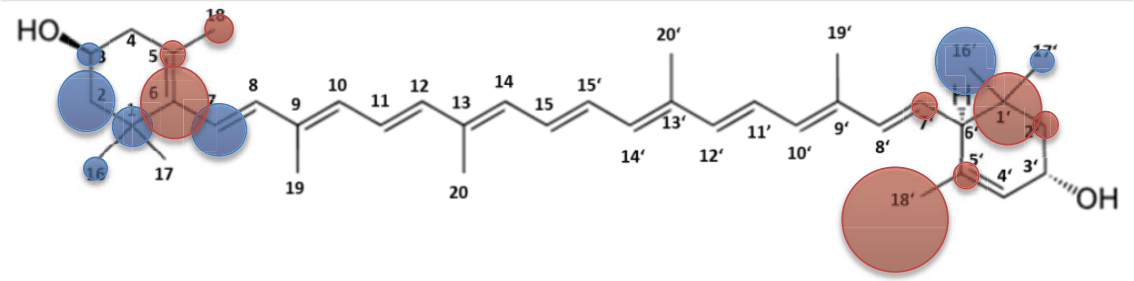

Figure 5.14 Lutein chemical structure mapping chemical shift differences δ between ^{13}C lutein-rLhcb1 in β-DM and lutein in $CDCl_3$ solution. Blue: downfield shifts; red: up-field shifts. The circle sizes represent the magnitudes of the shift differences.

DISCUSSION

From the crystal structure of LHCII, Lut1 is close to Chl *a*610 and Chl *a*612, while Lut2 is close to Chl *a*602 and Chl *a*603. The Chls *a*610 and *a*602 are close to the heads of the two luteins.
Both Chls *a*610 and *a*602 are ligated via an Arg-Glu ion pair in LHCII. The Arg-Glu ion pairs also have a structural role in stabilizing the two intersecting transmembrane helices of LHCII. In Sunku *et al.*, it was concluded that the Arg-Glu interactions do not change comparing the unquenched and quenched state of LHCII that was prepared respectively in *β*-DM and aggregated form [2]. Moreover, it was concluded that the orientation of Chl *a*610 and Chl *a*602 with respect to the ligating Arg does not change. From the results, it was predicted that any change in Lut-Chl interactions producing a quenched state, as has been proposed by several studies [9,15,29], should involve a movement of lutein relative to the adjacent Chls that are held in place in the protein.

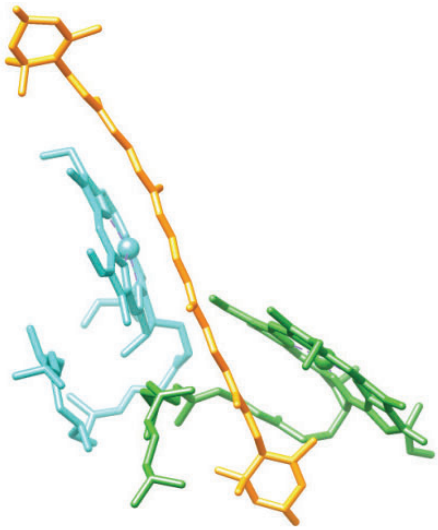

Figure 5.15 Pigments view of LHCII from spinach (PDB- 1RWT). Lut1 in orange, Chl a610 in green and Chl a612 in cyan.

From the representative structure shown in Figure 5.15 is visible how the lutein chain is almost parallel to Chl *a*612, while the methyl group from the lutein head is pointing toward the center of Chl *a*610. As Balevicius *at al.* predicted using simulation, the lutein moves accordingly to the protein functional state, which is translatable in a change of the interaction with both the Chls [30]. The luteins are stabilized by the stromal and luminal loops of LHCII that may undergo conformational changes in the quenched state. Indeed, the work of Sunku et al. showed a change in backbone conformation of an Arg located in the stromal loop [2]. Lut1 is stabilized by the helix D and the loop connecting helix A and D [1] (Figure 5.1). If any conformational change occurs in this loop region, the lutein position may be affected but not the Chls which are bound to the transmembrane helices A and B. Furthermore, chemical-shift changes that were observed in Chl a macrocycle

atoms (C4, C5 and C6) between the quenched and unquenched form of LHCII could tentatively be explained by a movement of Lut1 with respect to Chl *a*612 [1].

In support for the importance of carotenoids as one of the agents involved in the regulation of light harvesting in the photosystems under high-light conditions there is recent work from Balevicius *et al.* [30] Their study investigated the dependence of the energy-transfer inducing electronic coupling on the mutual orientation of Chl *a*612 and Lut1. Their model used a starting point in which Chl *a*612 is close to the middle section of the lutein (the C15=C15' bond in Figure 5.12), because that is the center of their transition density [30] and with the chlorine ring maximally parallel to the conjugation plane of the Car, which is a condition for efficient interaction due to the overlap of transition densities [31]. From the simulation, it is clear that the Chl-Car interaction is sensitive to the mutual orientation of the Car and Chl pigments [30]. The relative excitation transfer rate can be driven from excitation-preserving to quenching configurations within physical boundaries. This, according to them, supports the idea of Cars acting as one of the agents regulating energy density in the photosystems under high-light conditions, and presents the most realistic molecular switching pathway [30].

Our work reports for the first time on the structure of the luteins in LHCII in unquenched state, complementing the crystallographic structures of LHCII in the quenched state. Our finding that lutein C18' methyl NMR chemical shift is affected by ring-currents induced by Chl *a*610 (Lut1) and Chl *a*602 (Lut2) provides us now with a highly sensitive probe for comparing the distances and orientations of the lutein heads in unquenched and quenched states. With this approach, we can experimentally test if the photoprotective switch indeed involves a movement of lutein.

From the representative structure shown in Figure 5.15 it is visible how the lutein chain is almost parallel to Chl *a*612, while the methyl group from the lutein head is pointing toward the center of Chl *a*610. Balevicius *at al.* predicted that the lutein moves with respect to Chl *a* 612 accordingly to the protein functional state, which should be translatable in change of the interaction with both the Chls [30].

Moreover, the ring-current effects allow us to compare lutein structures of LHCII in *β*-DM with lutein in the LHCII crystal structures, as we can predict crystal-structure-based lutein-Chl ring-current shifts and compare those with the experimentally assigned chemical shifts of ^{13}C lutein-rLhcb1 in *β*-DM [32-34].

Although LHCII contains two luteins, we obtained only one set of lutein head correlations, with doubling of some of the peaks. This suggests that the two lutein molecules are similarly affected by the surrounding pigment-protein environment. Specifically, doubling of the C18' peaks indicates that the Lut1-Chl *a*610 and Lut2-Chl *a*602 interactions are similar and that there is a high degree of symmetry between the two pigment sites.

The appearance of lutein signals in the detergent sample only below 240 K indicates that at higher temperatures the lutein molecules undergo dynamic, internal motions on a (sub)microsecond timescale. As the lutein positions are correlated with their role as a light harvester or quencher, such dynamics might enable LHCII to switch between quenched and unquenched states.

CONCLUSIONS

In this work, we for the first time could detect the structure and dynamics of lutein in LHCII in unquenched state in a detergent environment. With this preliminary work, we opened the way for an investigation of the interaction between Lut1-Chl *a*610 (1), or Lut2-Chl *a*602, in quenched and unquenched states to test if the photoprotective switch involves a change in lutein-Chl interactions.

The C18' and H18' NMR chemical shifts are influenced by Chl ring currents and thereby can be used as markers that should be very sensitive to changes in the position and orientation of lutein in the protein. MAS NMR investigations of aggregated, quenched ^{13}C lutein-rLhcb1 are underway.

REFERENCES

1. Pandit A, Reus M, Morosinotto T, Bassi R, Holzwarth AR, de Groot HJ. An NMR comparison of the light-harvesting complex II (LHCII) in active and photoprotective states reveals subtle changes in the chlorophyll a ground-state electronic structures. *Biochim Biophys Acta*, 1827(6), 738-744 (2013).

2. Sunku K, de Groot HJ, Pandit A. Insights into the photoprotective switch of the major light-harvesting complex II (LHCII): a preserved core of arginine-glutamate interlocked helices complemented by adjustable loops. *J Biol Chem*, 288(27), 19796-19804 (2013).

3. Dall'Osto L, Lico C, Alric J, Giuliano G, Havaux M, Bassi R. Lutein is needed for efficient chlorophyll triplet quenching in the major LHCII antenna complex of higher plants and effective photoprotection in vivo under strong light. *BMC Plant Biol*, 6, 32 (2006).

4. Plumley FG, Schimdt W. Reconstitution of chlorophyll a/b light-harvesting complexes: Xanthophyll-dependent assembly and energy transfer. *Cell Biology*, 84, 146-150 (1987).

5. Formaggio E, Cinque G, Bassi R. Functional Architecture of the Major Light-harvesting Complex from Higher Plants. *J. Mol. Biol.* , 314, 1157-1166 (2001).

6. García-Plazaola JI, Matsubara S, Osmond CB. The lutein epoxide cycle in higher plants: its relationships to other xanthophyll cycles and possible functions. *Functional Plant Biology* 34(9), 759-773 (2007).

7. Horton P, Ruban AV, Walters RG. Regulationof Light Harvesting in green plants. *Annu. Rev. Plant Physiol. Plant Mol. Biol.*, 47, 655–684 (1996).

8. Natali A, Gruber JM, Dietzel L , Stuart MCA , van Grondelle R , Croce R. Light-harvesting Complexes (LHCs) Cluster Spontaneously in Membrane Environment Leading to Shortening of Their Excited State Lifetimes. *Jornal of biological chemistry* 291(32), 16730-16739 (2016).

9. Ruban AV, Berera R, Ilioaia C *et al.* Identification of a mechanism of photoprotective energy dissipation in higher plants. *Nature*, 450(7169), 575-578 (2007).

10. Pascal AA, Liu Z, Broess K *et al.* Molecular basis of photoprotection and control of photosynthetic light-harvesting. *Nature*, 436(7047), 134-137 (2005).

11. S. Bode, Quentmeier CC, Liao P-N, Hafi N, Barros T, Wilk L, Bittner F, and Wall PJ. On the regulation of photosynthesis by excitonic interactions between carotenoids and chlorophylls. *PNAS* 106(30), 12311–12316 (2009).

12. Miloslavina Y, Wehner A, Lambrev PH *et al.* Far-red fluorescence: a direct spectroscopic marker for LHCII oligomer formation in non-photochemical quenching. *FEBS Lett*, 582(25-26), 3625-3631 (2008).

13. Croce R, Weiss S, Bassi R. Carotenoid-binding Sites of the Major Light-harvesting Complex II of Higher Plants. *J. Mol. Biol.* 274(42), 29613–29623 (1999).

14. Standfuss J, van Scheltinga ACT, Lamborghini M, Kühlbrandt W. Mechanisms of photoprotection and nonphotochemical quenching in pea light-harvesting complex at 2.5 A resolution. *EMBO J*, 24(5), 919-928 (2005).

15. Liu Z, Hanchi Y, Wang K, Kuang T, Zhang J., Gui L, An X & Chang. W Crystal structure of spinach major lightharvesting complex at 2.72A˚ resolution. *NATURE*, 428, 2887-2292 (2004).

16. van Oort B, Marechal A, Ruban AV *et al.* Different crystal morphologies lead to slightly different conformations of light-harvesting complex II as monitored by variations of the intrinsic fluorescence lifetime. *Phys Chem Chem Phys*, 13(27), 12614-12622 (2011).

17. Wentworth M, Ruban AV, Horton P. Chlorophyll fuorescence quenching in isolated light harvesting complexes induced by zeaxanthin. *FEBS Lett*, (471), 71-74 (2000).

18. Wentworth M, Ruban AV, and Horton P. Kinetic Analysis of Nonphotochemical Quenching of Chlorophyll Fluorescence. 2. Isolated Light-Harvesting Complexes. *Biochemistry*, 40, 9902-9908 (2001).

19. Alpes H, Apell H-J, Knoll G, Plattner H and Riek R. Reconstitution of Na^+/K^+-ATPase into phosphatidylcholine vesicles by dialysis of nonionic alkyl maltoside detergents. *Biochimica et Biophysica Acta*, 946, 379-388 (1988).

20. Fung BM, Khitrin AK, Ermolaev K. An Improved Broadband Decoupling Sequence for Liquid Crystals and Solids. *Journal of Magnetic Resonance*, 142(1), 97-101 (2000).

21. Hartmann SR, Hahn EL. Nuclear Double Resonance in the Rotating Frame. *Physical Review*, 128(5), 2042-2053 (1962).

22. Andrew ER, Bradbury, A. and Eades, R. G. Nuclear magnetic resonance spectra from a crystal rotated at high speed. *Nature*, 182, 1659-1659; (1959).

23. Lowe IJ. Free Induction Decays of Rotating Solids. *Physical Review Letters*, 2 (7), 285-287 (1959).

24. Fung BM, Khitrin AK, and Ermolaev K. An Improved Broadband Decoupling Sequence for Liquid Crystals and Solids. *Journal of Magnetic Resonance*, 142, 97–101 (2000).

25. *http://chem.ch.huji.ac.il/nmr/techniques/2d/hetcor/hetcor.html*.

26. Tian D, Li T, Zhang R *et al.* Conformations and Intermolecular Interactions in Cellulose/Silk Fibroin Blend Films: A Solid-State NMR Perspective. *J Phys Chem B*, 121(25), 6108-6116 (2017).

27. Miao Y, Cross TA. Solid state NMR and protein-protein interactions in membranes. *Curr Opin Struct Biol*, 23(6), 919-928 (2013).

28. Mithu VS, Bakthavatsalam S, Madhu PK. ^{13}C-^{13}C homonuclear recoupling in solid-state nuclear magnetic resonance at a moderately high magic-angle-spinning frequency. *PLoS One*, 8(1), e50504 (2013).

29. Ilioaia C, Johnson MP, Liao PN *et al.* Photoprotection in plants involves a change in lutein 1 binding domain in the major light-harvesting complex of photosystem II. *J Biol Chem*, 286(31), 27247-27254 (2011).

30. Balevicius V Jr., Fox KF, Bricker WP *et al.* Fine control of chlorophyll-carotenoid interactions defines the functionality of light-harvesting proteins in plants. *Sci Rep*, 7(1), 13956 (2017).

31. Dreuw A, Fleming GR, Head-Gordon M. Role of electron-transfer quenching of chlorophyll fluorescence by carotenoids in non-photochemical quenching of green plants. *Biochemical Society Transactions*, 33(4), 858-862 (2005).

32. Abraham RJ, Smith KM. NMR Spectra of Porphyrins. 21. Applications of the Ring-Current Model to Porphyrin and Chlorophyll Aggregation1. *J. Am. Chem. Soc.*, 105, 5734-5741 (1983).

33. Janson TR, Kane AR, Sullivan JF, Knox K, and Kenney ME. The Ring-Current Effect of the Phthalocyanine Ring. *Journal of the American Chemical Society*, 91(19), 5210-5212 (1969).

34. Mizoguchi T, Sakamoto S, Koyama Y, Ogura K and Inagak F. The Structure of the Aggregate Form of Bacteriochlorophyll *c* Showing the Q, Absorption above 740 nm as Determined by the Ring-current Effects on ^{1}H and ^{13}C Nuclei and by ^{1}H-^{1}H Intermolecular NOE Correlations. *Photochemistry and Photobiology*, 67(2), 239-248 (1998).

35. Ragasa CY, Levida RM, Don MJ and Shen CC. Cytotoxic Isothiocyanates from *Moringa oleifera Lam* Seeds. *Philippine Science Letters*, 5(1) (2012).

36. La Fountain AM, Pacheco C, Prum RO, Frank HA. Nuclear magnetic resonance analysis of carotenoids from the burgundy plumage of the Pompadour Cotinga (Xipholena punicea). *Arch Biochem Biophys*, 539(2), 133-141 (2013).

37. Mathur A. Extraction, isolation and purification of Lutein, Zeaxanthin, Meso-Zeaxanthin and ß-Cryptoxanthin. CHAPTER-3.

A.5 Liquid and Solid-State NMR of lutein

^{13}C NMR lutein spectra were assigned accordingly to Ragasa *et al.* [35] while proton assignment is accordingly to [36,37] Even though this value comes from protein in $CDCl_3$ this is the best guess to start were to look for the pigment peaks. We expected indeed a shift of the ppm because the lutein in the protein is exposed to a different protein environment which reflect in shifts of the peaks.

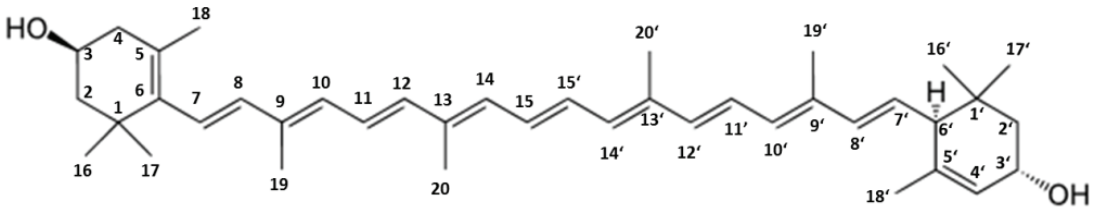

Figure A5. 1 Chemical structure of lutein.

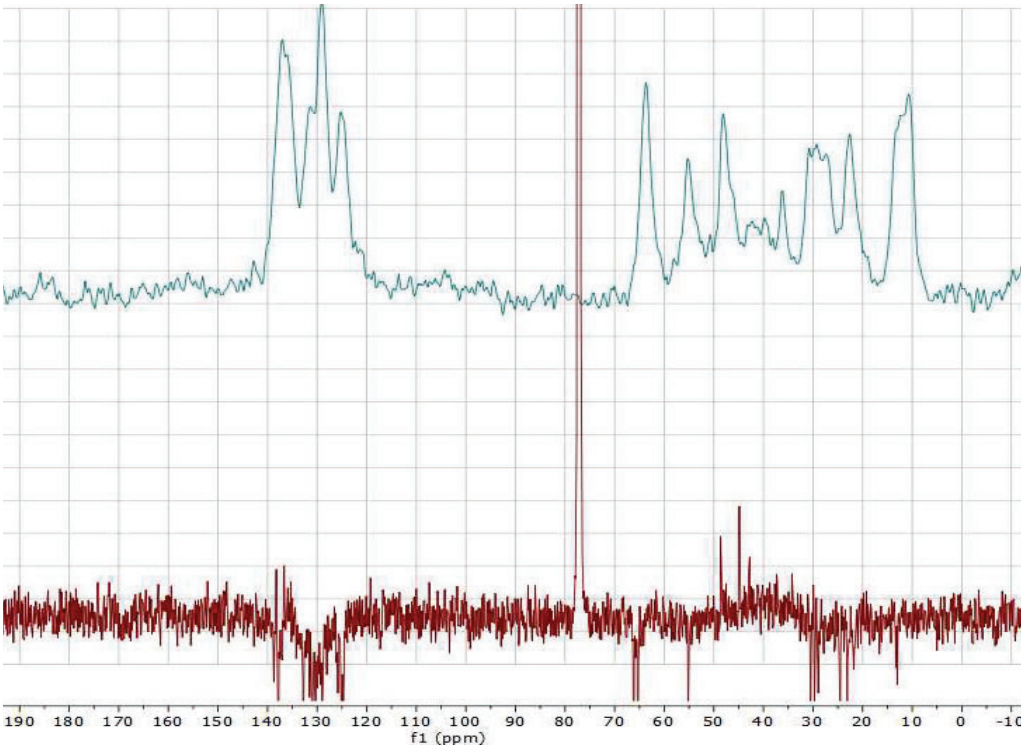

Figure A5.2 In blue 1D solid state NMR of na lutein powder compared with its liquid (dissolved in $CDCl_3$) NMR spectrum in red.

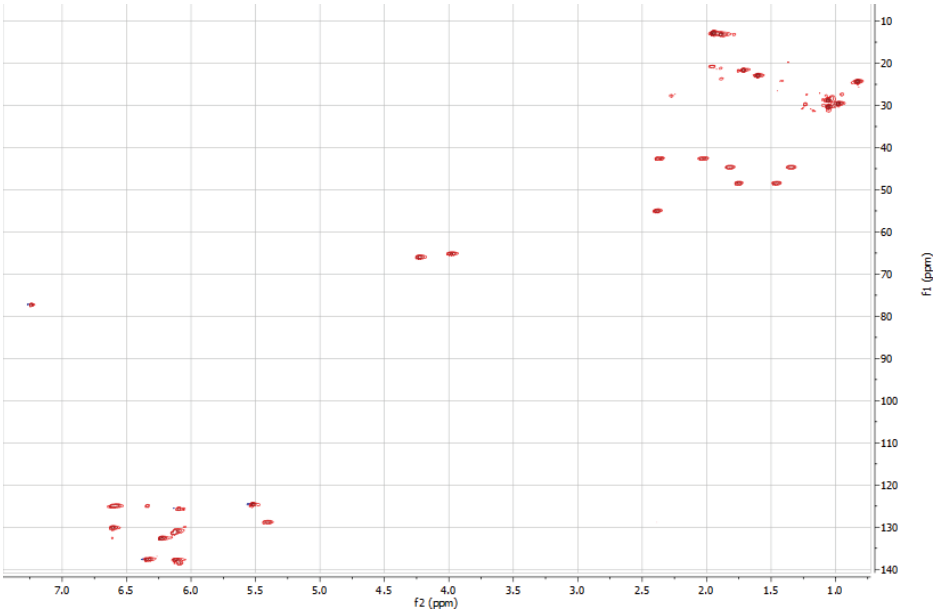

Figure A5.3 HSQC-EDETGP of lutein in $CDCl_3$. In blue -CH and -CH_3 and in red -CH_2 and -C.

Atoms	Functional group	^{13}C Chemical shift ppm	^{1}H Chemical shift ppm
x	CH	65.10	N/A
C_{16}	CH_3	28.70	1.07
C_{17}	CH_3	30.30	1.07
C_{18}	CH_3	21.60	1.74
C_{19}	CH_3	12.70	1.97
C_{20}	CH_3	12.70	1.967
$C_{20'}$	CH_3	12.80	1.967
$C_{19'}$	CH_3	13.10	1.91
$C_{18'}$	CH_3	22.90	1.64
$C_{16'}$	CH_3	29.50	0.85
$C_{17'}$	CH_3	24.70	0.99
$C_{1'}$	C	34.00	N/A
$C_{2'}$	CH_2	44.60	1.37 and 1.85
$C_{3'}$	CH (-OH)	65.90	N/A
$C_{4'}$	CH	124.50	6.64
$C_{5'}$	C	137.70	n/A
$C_{6'}$	CH	55.00	N/A
$C_{7'}$	CH	128.70	5,43
$C_{8'}$	CH	130.80	6.63
$C_{9'}$	C	135.10	N/A
$C_{10'}$	CH	137.60	6.26

$C_{11'}$	CH	124.80	6.64
$C_{12'}$	CH	137.70	6.36
$C_{13'}$	C	136.50	N/A-
$C_{14'}$	CH	132.60	6.14
$C_{15'}$	CH	130.10	6.63
C_{15}	CH	130.10	6.63
C_{14}	CH	132.60	6.26
C_{13}	C	136.40	N/A
C_{12}	CH	137.50	6.35
C_{11}	CH	124.90	6.64
C_{10}	CH	131.30	6.15
C_9	C	135.7	N/A
C_8	CH	138.50	6.15
C_7	CH	125.60	6.10
C_6	C	138.00	N/A
C_5	C	126.20	N/A
C_4	CH_2	42.50	2.04 AND 2.39
C_3	CH(-OH)	65.10	?
C_2	CH_2	48.40	1.45 and 1.77
C_1	C	37.10	N/A

Table A5.1 ^{13}C and ^{1}H chemical shift table of lutein in $CDCl_3$.

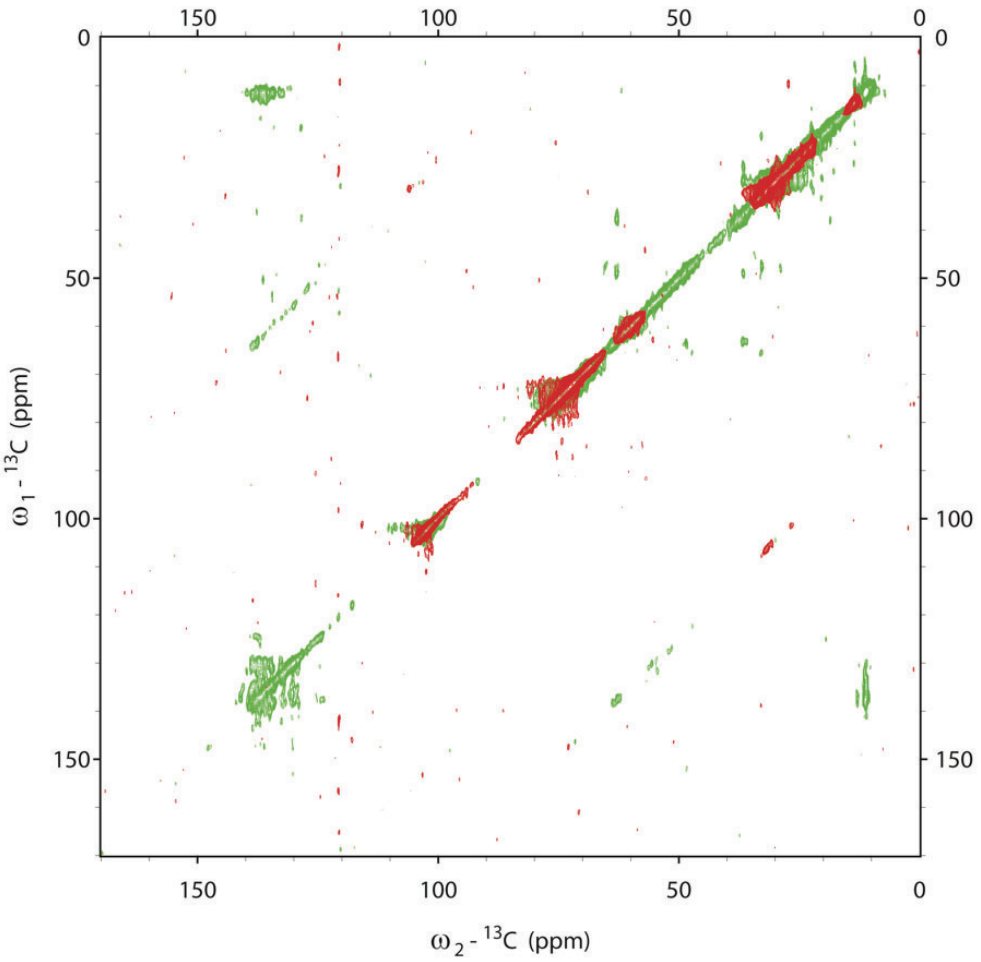

Figure A5.4 Overlaid ^{13}C-^{13}C PARIS NMR spectrum collected with 25ms mixing time. In red: NMR spectrum of β-DM and in green ^{13}C lutein-rLhcb1 in β-DM.

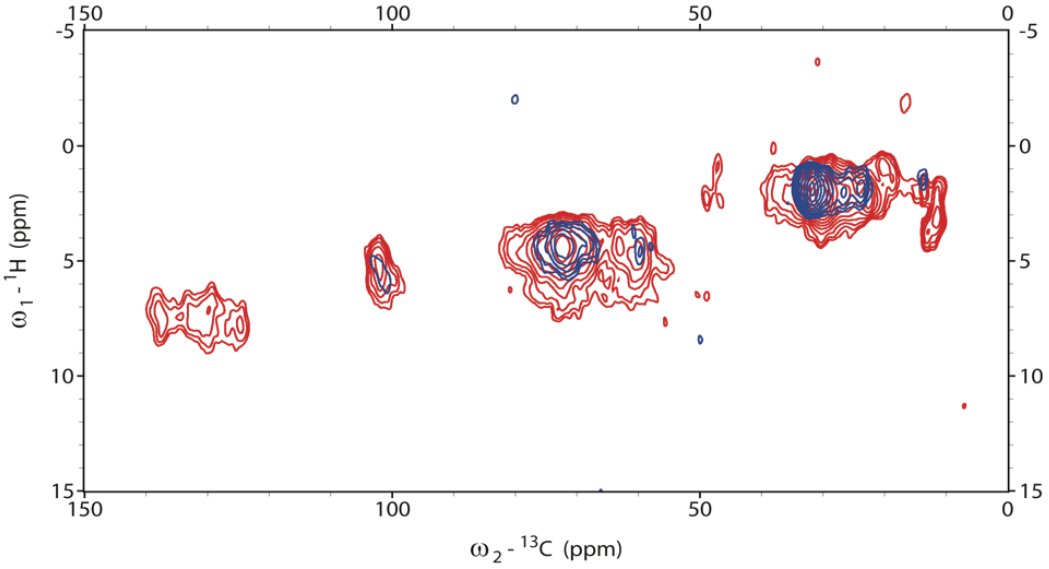

Figure A5.5 ^{1}H-^{13}C HETCOR spectra of the unquenched ^{13}C lutein-rLhcb1 in red and βDM in blue using 256 μs contact time.

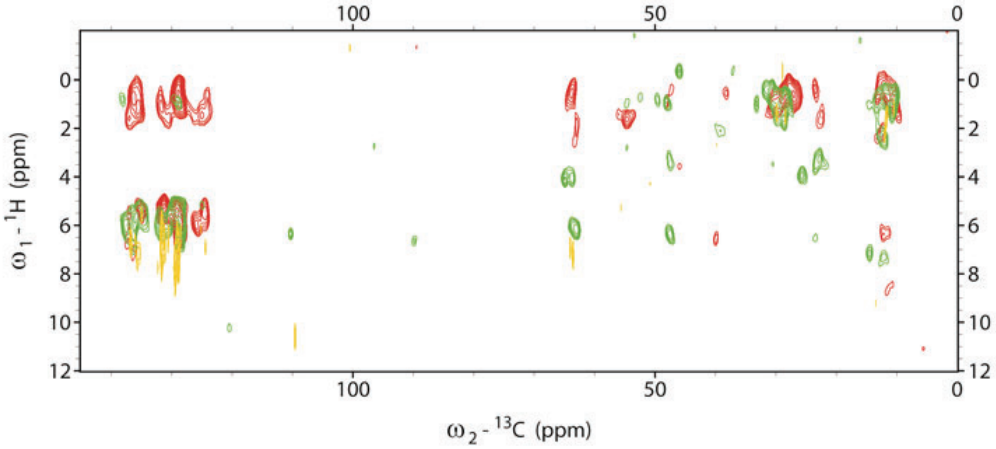

Figure A5.6 ^{1}H-^{13}C HETCOR spectra of ^{12}C lutein powder at different mixing time. In yellow 256 µs, in green 1024 µs and in red 3072 µs.

With the increase of the mixing time the correlation between ^{1}H and ^{13}C goes from 1 bond up to 3 bonds.